coatings

MDPI

Article

Design and Optimization of One-Dimensional TiO_2/GO Photonic Crystal Structures for Enhanced Thermophotovoltaics

Walid Belhadj [1,2,*], Abdelmajid Timoumi [1], Hassen Dakhlaoui [3] and Fahad Alhashmi Alamer [1]

1 Physics Department, College of Applied Science, Umm AL-Qura University, Makkah 24382, Saudi Arabia; aotemoume@uqu.edu.sa (A.T.); fahashmi@uqu.edu.sa (F.A.A.)
2 Laboratory Advanced Materials and Quantum Phenomena, Faculty of Sciences of Tunis, University Tunis El Manar, University Campus Farhat Hached Tunis B.P. 94–ROMMANA, Tunis 1068, Tunisia
3 Nanomaterials Technology Unit, Basic and Applied Scientific Research Center (BASRC), Physics Department, College of Science of Dammam, Imam Abdulrahman Bin Faisal University, P.O. Box 1982, Dammam 31441, Saudi Arabia; hbaldkhlaen@iau.edu.sa
* Correspondence: author: wbbelhadj@uqu.edu.sa

Abstract: In this paper, we theoretically explore the spectroscopic features of various one-dimensional photonic crystal (1D-PC)-based spectrally selective filters. The 1D-PC structure is composed of alternating layers of titanium dioxide (TiO_2) and graphene oxide (GO). Employing the transfer matrix method (TMM), the impacts of the incidence angle, the number, and thicknesses of TiO_2/GO layers in various 1D-PC stacks on the spectroscopic features of the filters are explored in detail. The proposed 1D-PC structures are designed for practical use for thermophotovoltaic (TPV) applications to act as filters that selectively transmit light below 1.78 µm to a GaSb photovoltaic cell, while light with longer wavelengths is reflected back to the source. The optimal design presented here consists of two Bragg quarter-wave 1D-PC filters with different central frequencies stacked to form a single structure. We demonstrate that our optimized 1D-PC filter exhibits a large omnidirectional stop band as well as a broad pass band and weak absorption losses. These features meet the fundamental exigencies to realize high-efficiency TPV devices. Additionally, we show that when integrated in a TPV system, our optimized filter leads to a spectral efficiency of 64%, a device efficiency of 39%, and a power density of 8.2 W/cm^2, at a source temperature of 1800 K.

Keywords: thermophotovoltaics; 1D-PC; selective filter; photonic band gap; device efficiency; transfer matrix

check for updates

Citation: Belhadj, W.; Timoumi, A.; Dakhlaoui, H.; Alhashmi Alamer, F. Design and Optimization of One-Dimensional TiO_2/GO Photonic Crystal Structures for Enhanced Thermophotovoltaics. *Coatings* **2022**, *12*, 129. https://doi.org/10.3390/coatings12020129

Academic Editor: Alicia de Andrés

Received: 11 December 2021
Accepted: 18 January 2022
Published: 24 January 2022

1. Introduction

Thermophotovoltaic (TPV) technology has received widespread attention due to its use in directly converting thermal energy radiated from a high-temperature source into electricity using photovoltaic (PV) cells [1–5]. A TPV device is composed of a heat source considered to be a perfect blackbody (BB), PV cells, and a selective filter. Unlike solar photovoltaic systems, the heat source in a TPV system is significantly closer to the PV diode, leading to a higher photon flux and power density as well as omnidirectional transfer of radiated power. In addition, TPV systems require PV cells with low band gap energy (E_g) semiconductors such as GaSb, InGaAs, and InGaAsSb because the temperature of the source is typically between 1000 and 1800 K [6]. Moreover, the closeness of the emitter to the PV cell authorizes photon recycling, leading to the enhancement of the device efficiency. The system efficiency and power density can be dramatically improved by the reflecting photon fraction having energies lower than the E_g of the PV cell to the source and transmitting photons with higher energies to the PV cell. The heat source absorbs the reflected light fraction and the energy can be recycled. Such energy recycling processes can be accomplished by employing a spectrally selective filter deposited on the PV cell-front, and/or backside reflectors deposited on its backside [7]. Until now, diverse highly efficient filter structures have been employed to enhance the performances of TPV devices. These filter structures comprised rugate and plasma filters [8–11] as well as distributed Bragg reflectors (DBRs) [12]. DBRs are layered structures in the form of 1D–PCs with a periodic refractive index along the normal to their surfaces [13,14]. Various types of spectrally selective filters based on 1D-PC structures with diverse constituent substances have been explored computationally and/or experimentally. Among these selective filters, we cite those comprising 1D-PC structures based on alternating layers of dielectric materials such as Si/SiO_2 [7,15,16] and TiO_2/SiO_2 [17,18] PC structures. The 1D metal-dielectric PCs composed of Ag/SiO_2 are also of note [19]. Babiker et al. [16] demonstrated 33.5% spectral efficiency at a source temperature of 1500 K for 1D Si/SiO_2 filter structures. In another study [7], a spectrally selective filter including ten periods of 1D-PC structure composed of Si/SiO_2 layers was optimized and fabricated. This device showed a power density of 2.1 W/cm^2 and spectral and system efficiencies of 40% and 24%, respectively. Mbakop et al. [20] conducted a comparative study between the performances of Si/SiO_2- and TiO_2/SiO_2-based 1D-PC structures. They demonstrated that for the same number of layers, the Si/SiO_2 structure exhibited a larger stop band in contrast to the TiO_2/SiO_2 structure. Recently, Gupta et al. [21] proposed a sub-band spectral filtering structure integrated in a TPV device with a GaSb PV diode. Their optimized structure demonstrated a prospect to reflect ~72% of the light radiated at a source temperature of 1500 K. More recently, Pirvaram et al. [22] employed a filtering structure composed of ZrO_2/ZrO_2-aerogel 1D-PC to ameliorate the efficiency of a TPV system based on GaSb PV cells. They reported that a power density of 8.5 W/cm^2 and spectral and system efficiencies of 46% and 33%, respectively, were obtained for their optimized filter at the emitter temperature of 1800 K.

In recent years, titanium dioxide (TiO_2) become one of the most attractive materials [23–27] that have been used to prepare functional 1D–PCs [28–32]. TiO_2 has a relatively large refractive index; therefore, when combined with materials with low refractive index, it results in a PBG. On the other hand, graphene oxide (GO) has excellent electrical and optical properties, good thermal conductivity, high mechanical strength, and a wide specific surface area [33,34]. GO is easily prepared and inexpensive, and it has a low refractive index, which is about 1.3 in the wavelength interval ranging from visible to near-infrared. Hence, the combination of GO with TiO_2 in a 1D-PC ensures a big difference between the refractive indices allowing a wide and high stop band.

In the present work, various 1D–PCs based on GO/TiO_2 stacked structures were designed and optimized for use as a spectrally selective filter for TPV applications. The TMM approach was employed to compute the optical response of these structures. The influence of several key parameters, such as number and thicknesses of the PC layers, and the incidence angle on the optical features of the filtering structures was explored in detail. Moreover, the optimized 1D-PC filter was integrated in a TPV system. Finally, the spectral and device efficiencies, as well as the power density was estimated using an ideal thermodynamic approach.

2. Model and Theory

In this study, a thermophotovoltaic (TPV) system was made up of a planar thermal source and a PV diode separated by an airgap of width L_0, as reported in [7,22] (see Figure 1). The source was assumed to be an ideal blackbody (BB) with a refractive index of $n_{BB} = 1.0$. The PV cell consisted of a GaSb cell with a refractive index of $n_{PV} = 3.9$ and gap energy of $E_g = 0.7$ eV, which corresponded to a cut-off wavelength of $\lambda_g = 1.78$ µm. A 1D-PC structure was positioned in front of the photodiode (see Figure 1) to enable the photons with wavelengths below λ_g to pass through it, while reflecting all other photons back to the blackbody source.

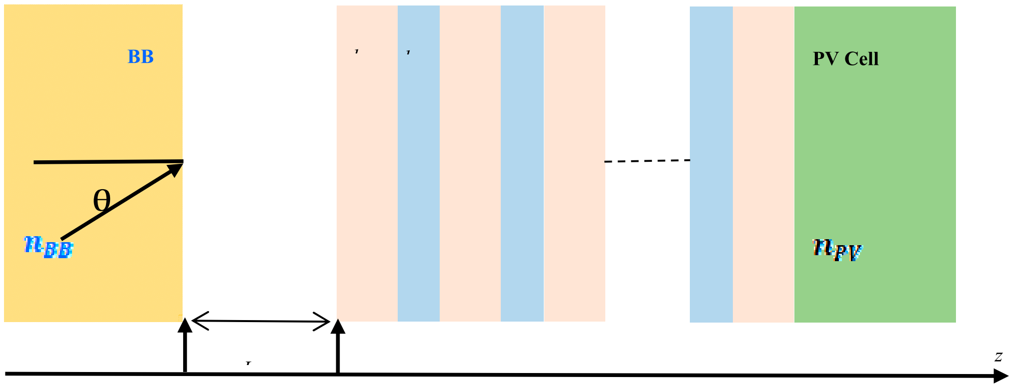

Figure 1. TPV system with blackbody emitter (BB) and a front side 1D-PC selective filter positioned in front of the PV diode that extends to +∞.

The electrical power density produced by a TPV device and its efficiency can be computed using an ideal thermodynamic approach, as detailed in [6,35]. Within the framework of this model, the photodiode was an ideal semiconductor where an electron–hole pair could be generated if the energy of the incident photon $\hbar\omega$ was greater than energy gap E_g. The power transmitted from a blackbody at temperature T_{BB} to the photodiode can be expressed according to the ideal thermodynamic model as follows:

$$P_{rad} = \int_0^\infty \frac{n_{BB}^2\omega^2}{4\pi^2c^2}\frac{\hbar\omega}{\exp\left(\frac{\hbar\omega}{k_BT_{BB}}\right)-1}\overline{T_{13}}(\omega)d\omega - \int_{\omega_g}^\infty \frac{n_{PV}^2\omega^2}{4\pi^2c^2}\frac{\hbar\omega}{\exp\left(\frac{\hbar\omega-eV}{k_BT_{PV}}\right)-1}\overline{T_{31}}(\omega)d\omega \quad (1)$$

where ω is the photon angular frequency, T_{BB} is the blackbody temperature, e is the electron charge, V is the voltage across the PV diode terminals, $\hbar$ is the reduced Planck's constant, and k_B is Boltzmann's constant. $\overline{T_{13}}$ and $\overline{T_{31}}$ are the average transmittance from the source to the photodiode and from the photodiode to the source, respectively. The amount of electrical power produced in the PV diode can be written as:

$$P_{PV} = eV\left\{\int_{\omega_g}^\infty \frac{n_{BB}^2\omega^2}{4\pi^2c^2}\frac{\hbar\omega}{\exp\left(\frac{\hbar\omega}{k_BT_{BB}}\right)-1}\overline{T_{13}}(\omega)d\omega - \int_{\omega_g}^\infty \frac{n_{PV}^2\omega^2}{4\pi^2c^2}\frac{\hbar\omega}{\exp\left(\frac{\hbar\omega-eV}{k_BT_{PV}}\right)-1}\overline{T_{31}}(\omega)d\omega\right\} \quad (2)$$

The first and second terms in the above equation represent the photon flux transferred from the source to the photodiode and from photodiode to the source, respectively. Hence, the device efficiency can be expressed as follows:

$$\eta_{TPV} = \frac{P_{PV}}{P_{rad}} \quad (3)$$

Moreover, in the case of a blackbody emitter, the spectral efficiency can be calculated according to [36] as follows:

Here $\overline{R_{13}}(\omega) = 1 - \overline{T_{13}}(\omega)$ is the average reflectance of the filter. $\eta_{spec}(T_{BB},\omega_g)$ specifies the ratio of the transmitted power below the cut-off wavelength to the total radiated power that attains the photodiode–filter system.

$$\eta_{spec}(T_{BB},\omega_g) = \frac{\int_0^{\omega_g} \frac{n_{BB}^2\omega^2}{4\pi^2c^2}\frac{\hbar\omega}{\exp\left(\frac{\hbar\omega}{k_BT_{BB}}\right)-1}\overline{T_{13}}(\omega)d\omega}{\int_0^\infty \frac{n_{BB}^2\omega^2}{4\pi^2c^2}\frac{\hbar\omega}{\exp\left(\frac{\hbar\omega}{k_BT_{BB}}\right)-1}\left(1-\overline{R_{13}}(\omega)\right)d\omega} \quad (4)$$

According to Planck's law, the spectral intensity of a blackbody source at temperature T is given by [37]:

$$I_{BB}(\lambda, T) = \frac{2\pi hc^2}{\lambda^5 \exp\left(\frac{hc}{\lambda k_B T}\right) - 1} \tag{5}$$

The transfer matrix method (TMM) [38] was used to simulate the optical features of our designed 1D-PC configurations. In this approach, each layer of the system was described by an interface matrix (I–matrix) and a propagation matrix (P–matrix). For the 1D layered structure, the P–matrix describing light propagation over the jth layer was represented according to [38] by a 2×2 matrix as follows:

$$P_j(d_j) = \begin{bmatrix} e^{-iK_{jz}d_j} & 0 \\ 0 & e^{iK_{jz}d_j} \end{bmatrix} \tag{6}$$

Meanwhile, the I–matrix that connects field components on either side of the j/k interface can be expressed according to [38] by the following matrix:

$$I_{j\to k} = \frac{1}{t_{j,k}} \begin{bmatrix} 1 & r_{j,k} \\ r_{j,k} & 1 \end{bmatrix} \tag{7}$$

where $t_{j,k}$ and $r_{j,k}$ are the Fresnel coefficients that are expressed for transverse electric (TE) and transverse magnetic (TM) polarizations as in [38]:

$$t_{j,k}^{TE} = \frac{2q_j}{q_j + q_k}, \quad t_{j,k}^{TM} = \frac{2\sqrt{\varepsilon_j}\sqrt{\varepsilon_k}q_j}{\varepsilon_k q_j + \varepsilon_j q_k} \tag{8}$$

$$r_{j,k}^{TE} = \frac{q_j - q_k}{q_j + q_k}, \quad r_{j,k}^{TM} = \frac{\varepsilon_k q_j - \varepsilon_j q_k}{\varepsilon_k q_j + \varepsilon_j q_k} \tag{9}$$

with $q_j = \sqrt{(\varepsilon_j - \varepsilon_a sin^2\theta)}$, where ε_a is the dielectric permittivity of the background medium and θ is the incidence angle.

The total transfer matrix can be written as:

$$S = \begin{bmatrix} S_{11} & S_{12} \\ S_{21} & S_{22} \end{bmatrix} = \prod_{j=1}^{N} \left(I_{j\to j+1} P_j(d_j)\right) I_{N\to N+1} \tag{10}$$

Finally, the reflectance R, transmittance T, and the absorbance A can be extracted from the Fresnel complex reflection and transmission coefficients as follows:

$$R = |r|^2 = \left|\frac{S_{21}}{S_{11}}\right|^2, \quad T = |t|^2 = \left|\frac{1}{S_{11}}\right|^2, \quad A = 1 - R - T. \tag{11}$$

The 1D-PC structures considered here are made of N alternating layers $[\mathrm{LH}]^N$ of high- and low-index materials with refractive indices n_H and n_L, respectively, deposited on a substrate with refractive index n_S. The thicknesses d_H and d_L of the high- and low-index material slabs were chosen to fulfill the Bragg quarter-wave stacks condition; $d_H n_H = d_L n_L = \lambda_0/4$, where λ_0 is the band gap central wavelength at normal incidence. It is well known that 1D–PCs can display total omnidirectional reflectance in the sense of an overlapping band gap at all incident angles, which can be employed to enhance the power conversion efficiency in TPV systems [39–41]. The wavelength λ_0 can be expressed in terms of the lower limit of the stop band which was chosen to be equal to the cut-off wavelength of the photodiode, according to [7].

$$\lambda_0 = \frac{1}{1 - \frac{2}{\pi}\sin^{-1}\left(\frac{n_H - n_L}{n_H + n_L}\right)} \lambda_g \tag{12}$$

3. Results and Discussion

In this study, the high- and low-index material layers were chosen to be titanium dioxide (TiO_2) with a refractive index n_H = 2.87 [42] and graphene oxide (GO) with a refractive index n_L = 1.328 [43], respectively. In our analysis, the spectroscopic features of the TiO_2/GO-based 1D-PC structures were investigated, as they related to the number and the thicknesses of PC layers, as well as the incidence angle of the radiated photons. The impact of each parameter among the above was also explored in detail. The basic parameters used in our calculation are summarized in Table 1.

Table 1. Refractive indices of the different materials used in our calculations and the corresponding references.

Material	Refractive Index	Reference
GaSb (PV diode)	$n_{PV} = 3.9$	[7]
TiO_2 (High-refractive-index material)	$n_H = 2.87$	[42]
GO (Low-refractive-index material)	$n_L = 1.328$	[43]
Blackbody (Ideal thermal emitter)	$n_{BB} = 1.0$	[7]

First, we explored the effect of the number of periods on the reflectance spectrum of our 1D-PC structure. As mentioned below, we chose the thicknesses of the layers to verify the Bragg quarter-wave stacks condition, $d_H n_H = d_L n_L = \lambda_0/4$, where λ_0 is the band gap central wavelength at normal incidence. To match the lower limit of the stop band to the photodiode cutoff wavelength, the central wavelength could be calculated according to Equation (12), so in this case λ_0 = 2.34 µm. Figure 2 displays the reflectance at normal incidence of 1D-PC structures with configurations $[LH]^N$ at λ_0 = 2.34 µm, N, extending from three to six. In general, one can obviously observe that the reflectance level of the structure increased by increasing the period number N. Particularly, the reflectance level along the photonic band gap (PBG) exceeded 99% for N = 5. However, the width of PBG narrowed slightly when increasing N from three to six layers. Hence, we chose N = 5 as the optimum value for the number of the PC periods. Note also that our 1D-PC filter displayed numerous considerable reflection peaks within the transmission band due to the change in the refractive-index profile. Such reflection ripples reduce the magnitude of radiated power attaining the photodiode in a TPV device [7].

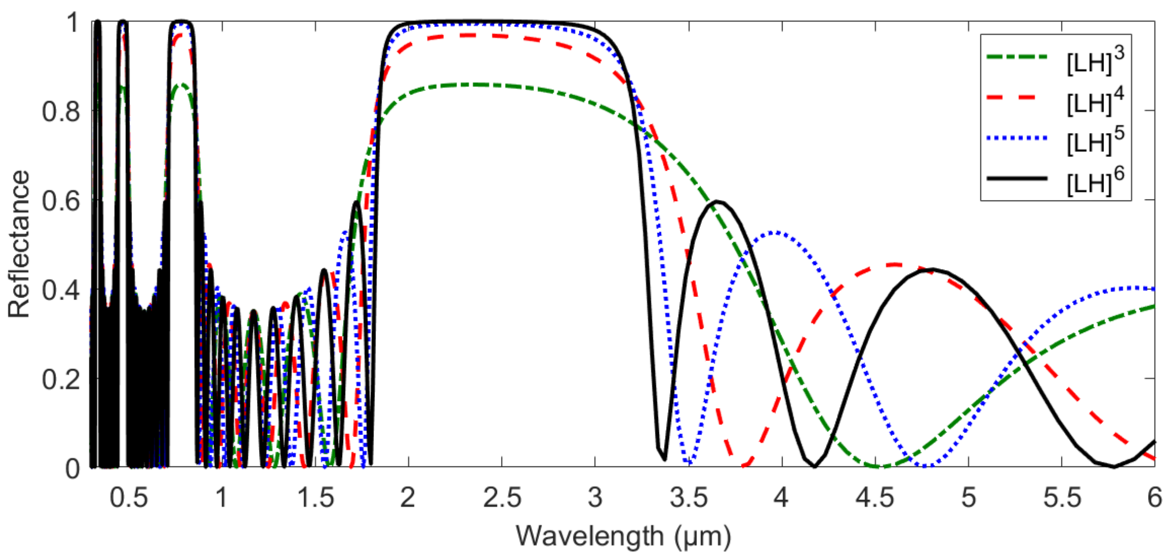

Figure 2. Reflectance spectra at normal incidence of the filter configuration $[LH]^N$ with different numbers of periods; the central wavelength is λ_0 = 2.34 µm.

To reduce the magnitude of the reflection peaks in the transmission band and ameliorate the efficiency of our structure, we followed the strategy proposed by O'Sullivan et al. [7]. The first layer in front to air could be reorganized into an anti-reflection coating by reducing the thickness dL to its half; thus, the structure would be $[L/2][H][LH]^4$. Figure 3 displays the reflectance spectra of the original structure ($[LH]^5$) as well as the adjusted one ($[L/2][H][LH]^4$). Obviously, the adjusted filter exhibited lower reflection level within the transmission band in contrast to the original one.

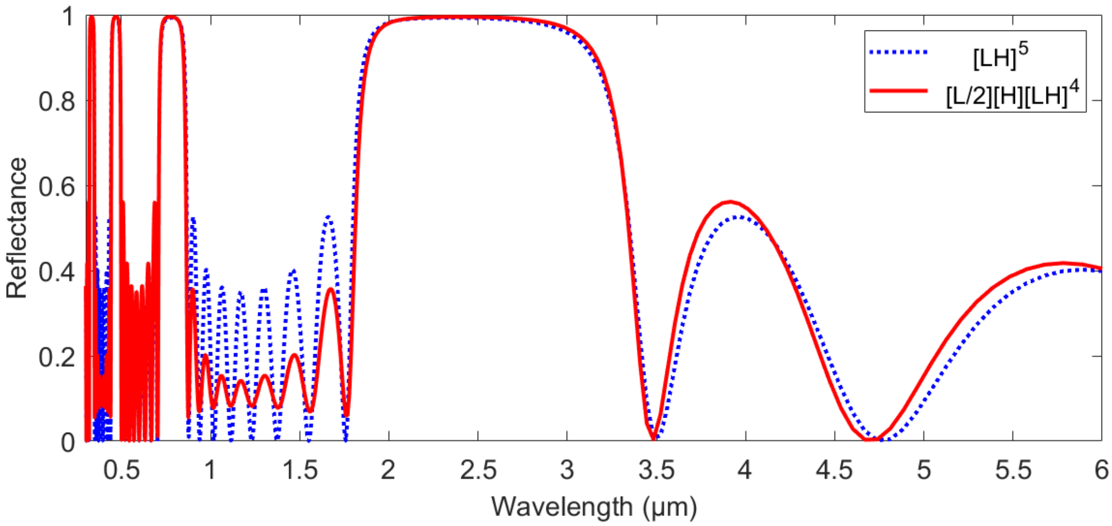

Figure 3. Reflectance spectra at normal incidence of the original filter configuration $[LH]^5$ and the adjusted structure $[L/2][H][LH]^4$; the central wavelength is λ_0 = 2.34 μm.

We continued our optimization by proceeding to obtain a larger PBG with the purpose of improving the efficiency of the device. It was reported in [4] that the PBG of a 1D-PC filter could be made wider by superposing together multiple filter configurations, having consecutive individual PBGs on top of each other. For this reason, we designed another 1D-PC filter having a lower-edge PBG to coincide with the upper edge of the above designed one. Since the spectral range of a PBG can be controlled by choosing the central wavelength of the Bragg stack, we optimized a second filter having a PBG consecutive to that of the above one. We found that the PBG of this filter was centered at about λ_0 = 3.3 μm. Figure 4 displays the normal-incidence reflectance spectra of our TiO_2/GO-based filters with the configuration $[LH]^5$ for two distinct values of the central wavelength λ_{01} = 2.34 μm ($[LH]^5(\lambda_{01})$) and λ_{02} = 3.3 μm ($[LH]^5(\lambda_{02})$). So, the thicknesses of the PC layers corresponding to the configuration $[LH]^5(\lambda_{01})$ are d_H = 203.8 nm and d_L = 440.5 nm, and those corresponding to the configuration $[LH]^5(\lambda_{02})$ are d_H = 287.5 nm and d_L = 621.2 nm. The reflectance spectra calculated for the double-stack filter configuration ($[LH]^5(\lambda_{01}).[LH]^5(\lambda_{02})$) as well as the normalized radiated intensity of the blackbody at 1600 K are displayed in Figure 4. From this figure, it is evident that both $[LH]^5(\lambda_{01})$ and $[LH]^5(\lambda_{02})$ configurations exhibited PBGs centered around λ_{01} = 2.34 μm and λ_{02} = 3.3 μm, respectively. As expected, the double-stack filter configuration exhibited a wider PBG region that extended over the two PBG ranges of the two individual filters.

Again, we needed to minimize the reflection oscillations in the pass band to ameliorate the efficiency of the double-stack filter; accordingly, we followed the strategy proposed in [4,7]. Thus, we considered several 1D-PC double-stack filters with various configurations and different anti-reflection coating (ARC) layers labeled as $[ARC]_1$ $[LH]^{N1}(\lambda_{01})\cdot[LH]^{N2}(\lambda_{02})$ $[ARC]_2$. Here $[ARC]_1$ and $[ARC]_2$ are anti-reflection coating layers at the beginning and end of the structure, respectively, and N_1 and N_2 are the numbers of periods in each stack within the structures. The normal-incidence reflectance spectra for these structures were calculated and are displayed in Figure 5. From this figure, it can be noted that wide PBGs with high reflectance levels were achieved for all configurations. The only thing that made a difference was the reflectance levels within the pass bands of the different structures. Among the proposed structures, we expect that the configuration $[L/2][H][LH]^4(\lambda_{01})\cdot[LH]^4(\lambda_{02})$ [L][H/2] is the most suitable to be used as spectral filter for TPV systems because it possessed the lowest reflectance level within the filter pass band.

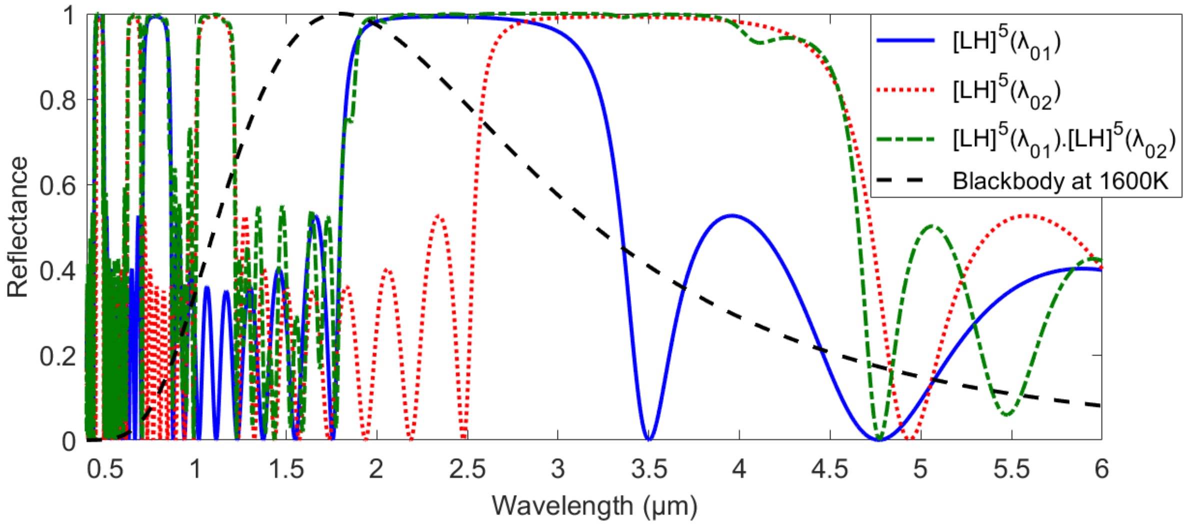

Figure 4. The normalized radiated intensity of the blackbody at 1600 K and the reflectance spectra at normal incidence of the filter configuration $[LH]^5$ for two values of the central wavelength λ_{01} = 2.34 μm and λ_{02} = 3.3 μm.

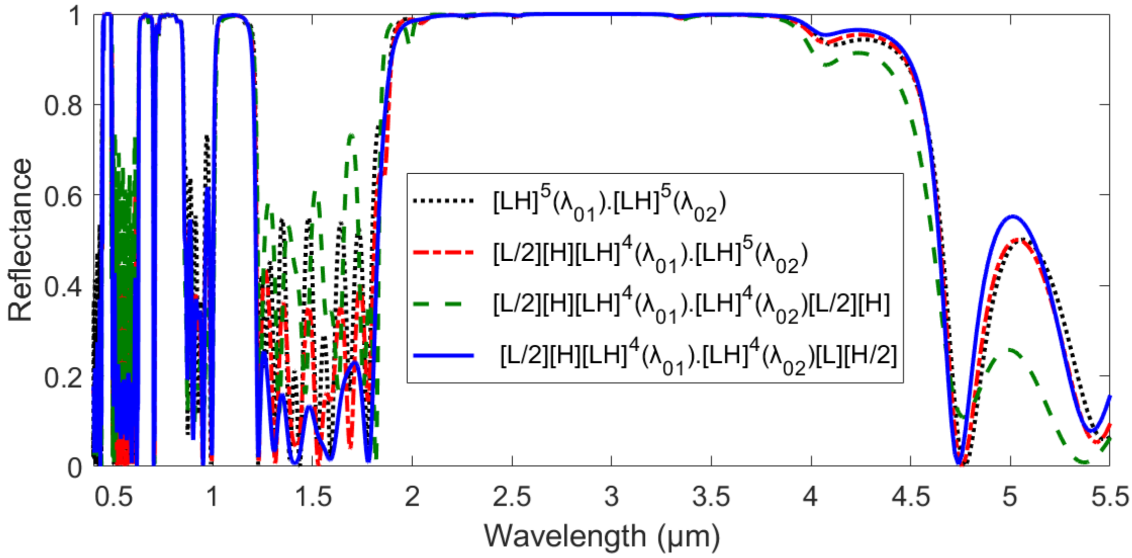

Figure 5. The normal-incidence reflectance spectra of double-stack filter with various configurations and different anti-reflection coating layers.

We continued our analysis by exploring the dependency of the reflectance spectra on the incidence angle. At oblique incidence, the spectroscopic behaviors of the filter depend on the polarization state of the incident light. So, both transverse electric (TE) and transverse magnetic (TM) polarizations were examined. Reflectance spectra for various incidence angles for a double-stack filter configuration $[L/2][H][LH]^4(\lambda_{01})\cdot[LH]^4(\lambda_{02})$ [L][H/2] are displayed in Figure 6 for both TE and TM modes. This figure shows that TE and TM modes manifested an identical stop band for normally incident waves. However, for waves with oblique incidence angles, the optical response of the structure was significantly affected.

This behavior is due to the fact that the interference condition related to the periodic refractive-index profile, which changed with the incidence angle. Moreover, for TM and TE waves the upper edge of the PBG shifted towards shorter wavelengths. According to Figure 6, we can also note that for TM mode the stop band narrowed when the incidence angle increased, and the upper edge shifted downward to the lower wavelengths more quickly than for TE mode. Another interesting point is that in the case of TM mode the reflectance level inside the PBG decreased when increasing the incidence angle, while it remained high in the case of TE mode. These behaviors could be explained by the fact that in case of TM waves, the surface current was proportional to the z component of the wave-vector (k_z), so the gap narrowed and began to disappear. However, in the case of TE waves, the surface current was inversely proportional to k_z, so, the gap broadened with the increase of θ, and the stop band persisted even for grazing incidences. In addition, the TM stop band began to disappear at an incidence angle of approximately 80°, while in the case of TE polarization, the stop band persisted even for incidence angles greater than 80°. Broadly, the reflectance behaviors in Figure 6, calculated for oblique incidences, show that the designed TiO_2/GO-based 1D-PC preserved reasonable levels of spectroscopic features even at an incidence angle of approximately 80°, maintaining both the critical stop-band and pass-band characteristics.

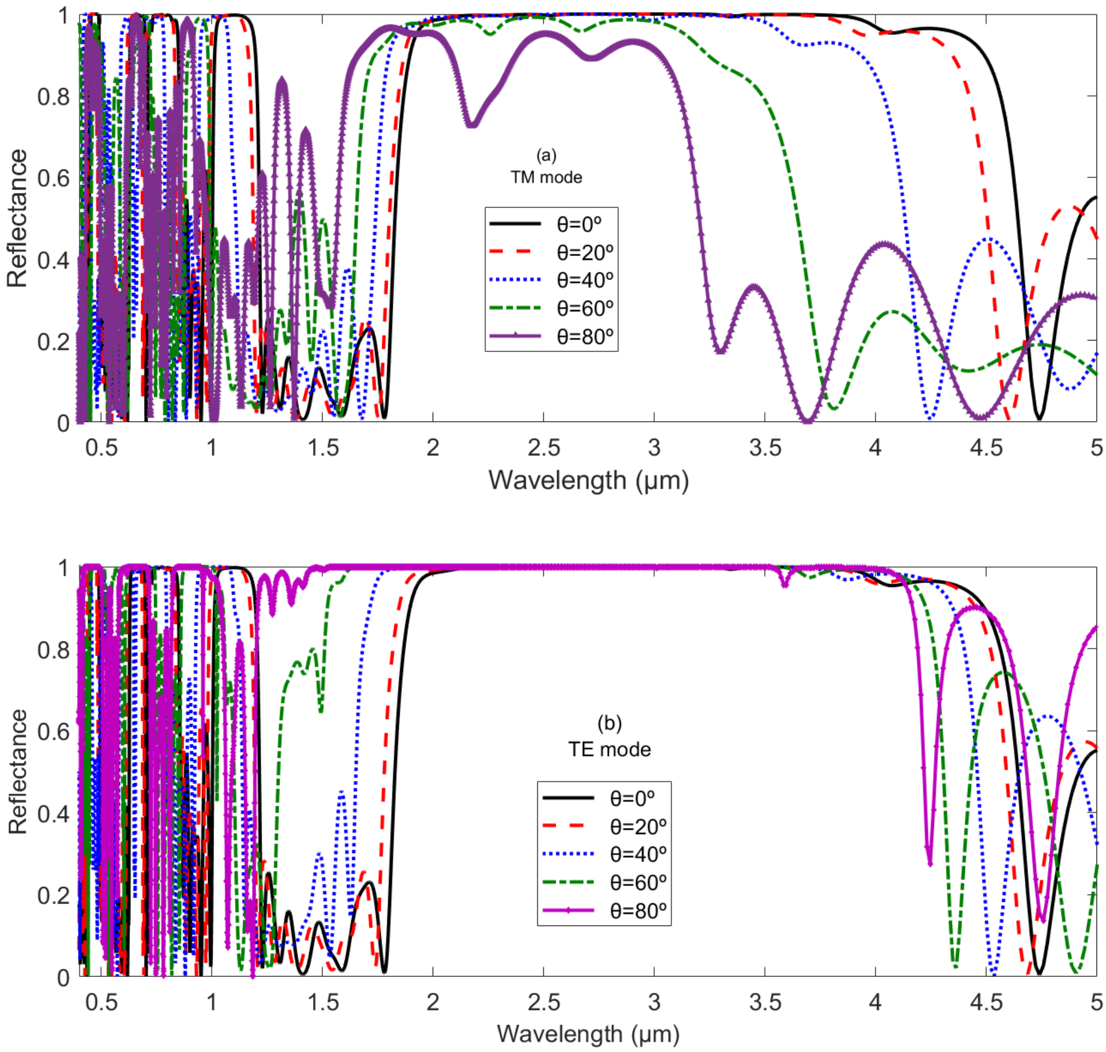

Figure 6. Reflectance spectra of double-stack filter configuration [L/2][H][LH]^4(λ_{01})·[LH]^4(λ_{02}) [L][H/2] at various incidence angles for (**a**) TM mode and (**b**) TE polarizations.

To estimate the ability of the different 1D-PC designs (detailed above) to ameliorate the performances of the TPV devices, the power density and efficiency versus the emitter temperature were computed for each of these configurations and the results are displayed in Figure 7. This figure reveals that the TPV device integrating single-stack filter configuration ([L/2][H][LH]^4(λ_{01})) exhibited somewhat higher power density in contrast to those with double-stack configurations. This was predictable since this structure had the lowest reflectance levels within the transmission band.

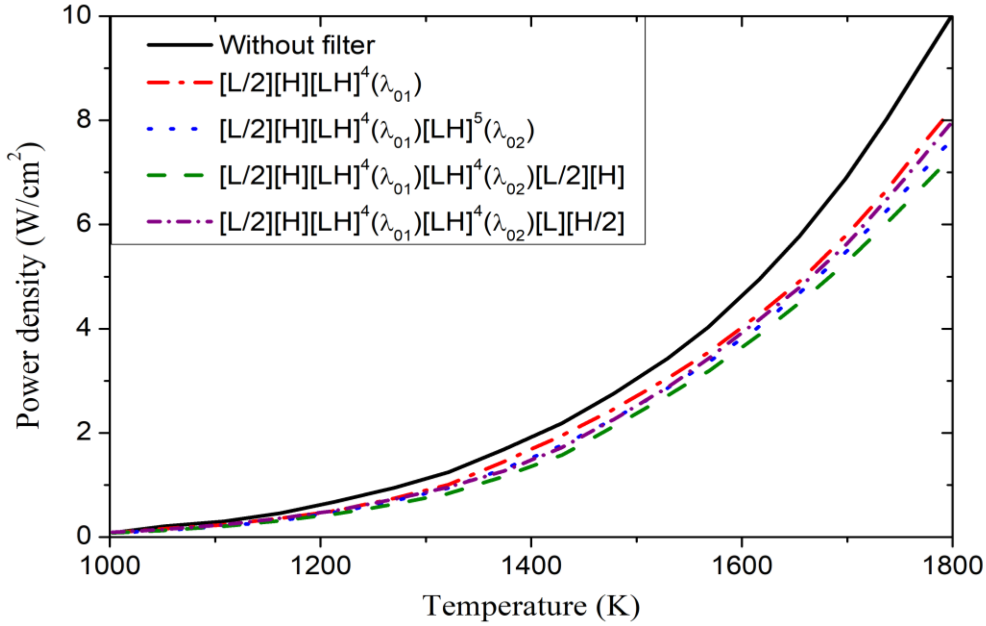

(**a**)

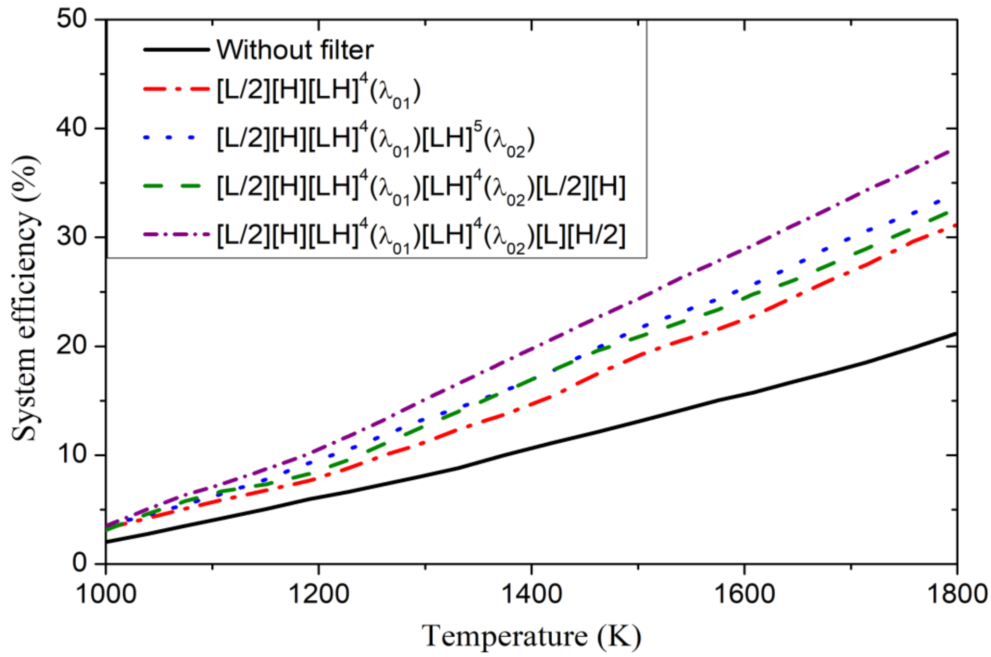

(**b**)

Figure 7. Calculated power density (**a**) and system efficiency (**b**) of GaSb TPV device vs. the source temperature for various filter configurations.

In fact, according to Equation (2), we can deduce that at specific temperatures a higher in-band transmittance (lower in-band reflectance) was associated with a higher power density. Thus, as the single-stack filter possessed a lower in-band reflectance than the double-stack configurations, the power density was higher in the single-stack structure. Nevertheless, the single-stack structure suffered from weak efficiency because of its tight stop band, and we see from Figure 7b that the double-stack structures exhibited higher efficiencies. Among the considered double-stack structures, the one with the configuration [L/2][H][LH]^4(λ_{01})·[LH]^4(λ_{02}) [L][H/2] exhibited higher power density and efficiency.

Spectral efficiency is another index ordinarily employed to measure the performances of TPV devices integrating 1D-PC filtering structures. Subsequently, the spectral efficiencies (η_{spec}) of our 1D-PC designs with single and double-stack configurations were calculated, and we present the results in Figure 8. The simulated spectral efficiencies versus source temperature suggest that the double-stack configuration [L/2][H][LH]^4(λ_{01})·[LH]^4(λ_{02}) [L][H/2] exhibited the best spectral efficiency compared to other configurations. So, it manifested a better trade-off among efficiency, power density, and spectral efficiency.

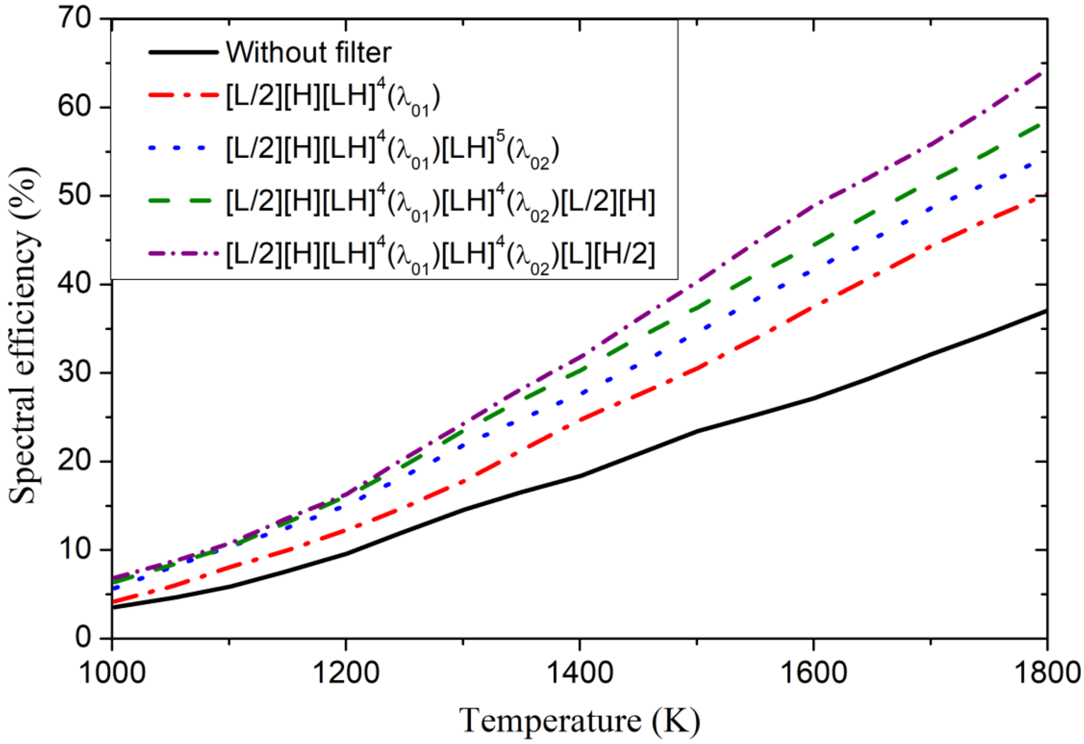

Figure 8. Spectral efficiencies of various 1D-PC filter configurations for GaSb diode with λ_g = 1.78 µm.

4. Conclusions

Using the TMM method, we investigated the spectroscopic properties of TiO_2/GO-based 1D-PC structures as spectrally selective filters for TPV applications. The 1D-PC filters presented here were designed and optimized to selectively reflect and transmit the out-of-band and in-band light fractions. We found that the stacking of two 1D-PC filters with suitable periods could simultaneously lead to a wide omnidirectional stop band with a broad pass band and weak absorption losses. Consequently, our proposed structure met the main requirements to ensure high efficiency and high power density in the case of TPV systems. The optimal design displayed in our analysis consists of a double-stack 1D-PC structure, denoted as [L/2][H][LH]^4(λ_{01})·[LH]^4(λ_{02}) [L][H/2]. The performance improvements accomplished by employing the designed filters in a perfect TPV device, including a GaAs PV diode and source in a parallel configuration, were specified. We demonstrated that, when integrated in a perfect TPV device at a source temperature of ~1800 K, our optimized double-stack configuration augmented the spectral efficiency from 32% to 64%. Moreover, compared to the situation without a filter, the power density of the TPV device was reduced from 10 to 8.2 W/cm^2, while the system efficiency was raised from 21% to 39%.

Author Contributions: Conceptualization, W.B., A.T., H.D. and F.A.A.; methodology, W.B. and A.T.; software, W.B. and H.D.; validation, W.B., A.T., H.D. and F.A.A.; formal analysis, W.B., A.T., H.D. and F.A.A.; investigation, W.B., A.T., H.D. and F.A.A.; resources, W.B.; data curation, W.B. and A.T.; writing—original draft preparation, W.B.; writing—review and editing, W.B., A.T., H.D. and F.A.A.; visualization, W.B., A.T., H.D. and F.A.A.; supervision, W.B.; project administration, W.B.; funding acquisition, W.B. All authors have read and agreed to the published version of the manuscript.

Funding: This research was funded by the Deanship of Scientific Research at Umm Al-Qura University, Makkah, Saudi Arabia, grant code: 19-SCI-1-01-0017.

Institutional Review Board Statement: Not applicable.

Informed Consent Statement: Not applicable.

Data Availability Statement: Data are contained within the article.

Acknowledgments: The authors would like to thank the Deanship of Scientific Research at Umm Al-Qura University, Makkah, Saudi Arabia for supporting this work by Grant Code: 19-SCI-1-01-0017.

Conflicts of Interest: The authors declare no conflict of interest.

References

1. Coutts, T.J. An overview of thermophotovoltaic generation of electricity. *Sol. Energy Mater. Sol. Cells* **2001**, *66*, 443–452. [CrossRef]
2. Fraas, L.M.; Avery, J.E.; Huang, H.X.; Martinelli, R.U. Thermophotovoltaic system configurations and spectral control. *Semicond. Sci. Technol.* **2003**, *18*, S165–S173. [CrossRef]
3. Burger, T.; Sempere, C.; Roy-Layinde, B.; Lenert, A. Present Efficiencies and Future Opportunities in Thermophotovoltaics. *Joule* **2020**, *4*, 1660–1680. [CrossRef]
4. Rostami, M.; Pirvaram, A.; Talebzadeh, N.; O'Brien, P.G. Numerical evaluation of one-dimensional transparent photonic crystal heat mirror coatings for parabolic dish concentrator receivers. *Renew. Energy* **2021**, *171*, 1202–1212. [CrossRef]
5. Kazim, A.H.; Salman, A.; Khan, A.B.; Shaukat, U.; Shabbir, A. Optimization of Thermophotovoltaic Power System with a Spectrally Controlled Multi-Concentric Emitter. *J. Energy Resour. Technol.* **2022**, *144*, 1–41. [CrossRef]
6. Zenker, M.; Heinzel, A.; Stollwerck, G.; Ferber, J.; Luther, J. Efficiency and power density potential of combustion-driven ther-mophotovoltaic systems using GaSb photovoltaic cells. *IEEE Trans. Electron. Devices* **2001**, *48*, 367–376. [CrossRef]
7. O'Sullivan, F.; Celanović, I.; Jovanović, N.; Kassakian, J.; Akiyama, S.; Wada, K. Optical characteristics of one-dimensional Si/SiO_2 photonic crystals for thermophotovoltaic applications. *J. Appl. Phys.* **2005**, *97*, 033529. [CrossRef]
8. Ilyas, S.; Böcking, T.; Kilian, K.; Reece, P.J.; Gooding, J.; Gaus, K.; Gal, M. Porous silicon based narrow line-width rugate filters. *Opt. Mater.* **2007**, *29*, 619–622. [CrossRef]
9. Ortabasi, U.; Bovard, B. Rugate technology for thermophotovoltaic applications: A new approach to near perfect filter performance. *AIP Conf. Proc.* **2003**, *653*, 249–258.
10. Ehsani, H.; Bhat, I.; Borrego, J.; Gutmann, R.; Brown, E.; Dziendziel, R.; Freeman, M.; Choudhury, N. Optical properties of de-generately doped silicon films for applications in thermophotovoltaic systems. *J. Appl. Phys.* **1997**, *81*, 432–439. [CrossRef]
11. Rahmlow, T.; Lazo-Wassem, J.; Gratrix, E.; Fourspring, P.; DePoy, D.; Azarkevich, J. Engineering Spectral Control Using Front Surface Filters for Maximum TPV Energy Conversion System Performance. In Proceedings of the 2nd International Energy Conversion Engineering Conference, American Institute of Aeronautics and Astronautics (AIAA), Providence, RI, USA, 16 August 2004; p. 5678.
12. Isabella, O.; Dobrovolskiy, S.; Kroon, G.; Zeman, M. Design and application of dielectric distributed Bragg back reflector in thin-film silicon solar cells. *J. Non-Cryst. Solids* **2012**, *358*, 2295–2298. [CrossRef]
13. Meade, R.D.V.E.; Johnson, S.G.; Winn, J.M. The Multilayer Film: A One-Dimensional Photonic Crystal. *Gruyter* **2008**, 44–65.
14. Rostami, M.; Talebzadeh, N.; O'Brien, P.G. Transparent photonic crystal heat mirrors for solar thermal applications. *Energies* **2020**, *13*, 1464. [CrossRef]
15. Mao, L.; Ye, H. New development of one-dimensional Si/SiO_2 photonic crystals filter for thermophotovoltaic applications. *Renew. Energy* **2010**, *35*, 249–256. [CrossRef]
16. Babiker, S.G.; Shuai, Y.; Sid-Ahmed, M.O.; Xie, M.; Sid-Ahmed, M.O. Design of a one Dimensional Si/SiO_2 photonic crystals filter for thermophotovoltaic application. *INMIC* **2013**, 177–181. [CrossRef]
17. Mbakop, F.K.; Djongyang, N.; Raïdandi, D. One–dimensional TiO_2/SiO_2 photonic crystal filter for thermophotovoltaic applications. *J. Eur. Opt. Soc. Rapid Publ.* **2016**, *12*, 23. [CrossRef]
18. Mbakop, F.K.; Djongyang, N.; Ejuh, G.W.; Raïdandi, D.; Woafo, P. Transmission of light through an optical filter of a one-dimensional photonic crystal: Application to the solar thermophotovoltaic system. *Phys. B Condens. Matter* **2017**, *516*, 92–99. [CrossRef]

19. Zhang, C.; Tang, L.; Liu, Y.; Liu, Z.; Liu, W.; Qiu, K. A novel thermophotovoltaic optical cavity for improved irradiance uniformity and system performance. *Energy* **2020**, *195*, 116962. [CrossRef]
20. Mbakop, F.K.; Tom, A.; Dadj'e, A.; Vidal, A.K.; Djongyang, N. One-dimensional comparison of TiO_2/SiO_2 and Si/SiO_2 photonic crystals filters for thermophotovoltaic applications in visible and infrared. *Chin. J. Phys.* **2020**, *67*, 124–134. [CrossRef]
21. Gupta, M.V.N.S.; Ameen, E.; Unnikrishnakurup, S.; Balasubramaniam, K.; Veeraragavan, A.; Pesala, B. Spectral filtering of sub-bandgap radiation using all-dielectric gratings for thermophotovoltaic applications. *J. Photon. Energy* **2021**, *11*, 015501. [CrossRef]
22. Pirvaram, A.; Talebzadeh, N.; Rostami, M.; Leung, S.N.; O'Brien, P.G. Evaluation of a ZrO_2/ZrO_2-aerogel one-dimensional photonic crystal as an optical filter for thermophotovoltaic applications. *Therm. Sc. Eng. Prog.* **2021**, *25*, 100968. [CrossRef]
23. Serga, V.; Burve, R.; Krumina, A.; Romanova, M.; Kotomin, E.; Popov, A. Extraction–Pyrolytic Method for TiO_2 Polymorphs Production. *Crystals* **2021**, *11*, 431. [CrossRef]
24. Tsebriienko, T.; Popov, A.I. Effect of Poly(Titanium Oxide) on the Viscoelastic and Thermophysical Properties of Interpenetrating Polymer Networks. *Crystals* **2021**, *11*, 794. [CrossRef]
25. Lin, Y.-P.; Isakoviča, I.; Gopejenko, A.; Ivanova, A.; Začinskis, A.; Eglitis, R.I.; D'yachkov, P.N.; Piskunov, S. Time-Dependent Density Functional Theory Calculations of N- and S-Doped TiO_2 Nanotube for Water-Splitting Applications. *Nanomaterials* **2021**, *11*, 2900. [CrossRef] [PubMed]
26. Belhadj, W.; Timoumi, A.; Alamer, F.A.; Alsalmi, O.H.; Alamri, S.N. Experimental study and theoretical modeling of coat-ing-speed-dependent optical properties of TiO_2-graphene-oxide thin films. *Results Phys.* **2021**, *30*, 104867. [CrossRef]
27. Timoumi, A.; Albetran, H.M.; Alamri, H.R.; Alamri, S.N.; Low, I.M. Impact of annealing temperature on structural, morpho-logical and optical properties of GO-TiO_2 thin films prepared by spin coating technique. *Superlattices Microstruct.* **2020**, *139*, 106423. [CrossRef]
28. Guo, M.; Su, H.; Zhang, J.; Liu, L.; Fu, N.; Yong, Z.; Huang, H.; Xie, K. Broadband and omnidirectional light harvesting enhancement in photovoltaic devices with aperiodic TiO_2 nanotube photonic crystal. *J. Power Sources* **2017**, *345*, 12–20. [CrossRef]
29. Zheng, X.; Li, D.; Li, X.; Chen, J.; Cao, C.; Fang, J.; Wang, J.; He, Y.; Zheng, Y. Construction of ZnO/TiO_2 photonic crystal heterostructures for enhanced photocatalytic properties. *Appl. Catal. B Environ.* **2015**, 408–415. [CrossRef]
30. González-García, L.; Colodrero, S.; Míguez, H.; González-Elipe, A.R. Single-step fabrication process of 1-D photonic crystals coupled to nanocolumnar TiO_2 layers to improve DSC efficiency. *Opt. Express* **2015**, *23*, A1642–A1650. [CrossRef] [PubMed]
31. Deng, Y.; Ma, Z.; Ren, F.; Wang, G. Improved photoelectric performance of DSSCs based on TiO_2 nanorod array/Ni-doped TiO_2 compact layer composites film. *J. Solid State Electrochem.* **2019**, *23*, 3031–3041. [CrossRef]
32. Wang, L.; Zhang, S.; Lutkenhaus, J.L.; Chu, L.; Tang, B.; Lia, S.; Ma, W. All nanoparticle-based P(MMA–AA)/TiO_2 one-dimensional photonic crystal films with tunable structural colors. *J. Mater. Chem. C* **2017**, *5*, 8266–8272. [CrossRef]
33. Narayana, M.V.; Jammalamadaka, S.N. Tuning Optical Properties of Graphene Oxide under Compressive Strain Using Wet Ball Milling Method. *Graphene* **2016**, *05*, 73–80. [CrossRef]
34. Diamantopoulou, A.; Sakellis, E.; Gardelis, S.; Tsoutsou, D.; Glenis, S.; Boukos, N.; Dimoulas, A.; Likodimos, V. Advanced Photocatalysts Based on Reduced Nanographene Oxide-TiO_2 Photonic Crystal Films. *Materials* **2019**, *12*, 2518. [CrossRef] [PubMed]
35. Celanović, I.; Ilak, M.; Kassakian, J.; Perreault, D.; O'Sullivan, F. Design and optimization of one-dimensional photonic crystals for thermophotovoltaic applications. *Opt. Lett.* **2004**, *29*, 863–865. [CrossRef]
36. Baldasaro, P.F.; Raynolds, J.E.; Charache, G.W.; Depoy, D.M.; Ballinger, C.T.; Donovan, T.; Borrego, J.M. Thermodynamic analysis of thermophotovoltaic efficiency and power density tradeoffs. *J. Appl. Phys.* **2001**, *89*, 3319–3327. [CrossRef]
37. Yeng, Y.X.; Chan, W.R.; Rinnerbauer, V.; Joannopoulos, J.D.; Soljačić, M.; Celanovic, I. Performance analysis of experimentally viable photonic crystal enhanced thermophotovoltaic systems. *Opt. Express* **2013**, *21*, A1035–A1051. [CrossRef]
38. Hoenders, B.J.; Bertolotti, M. Coherence theory of electromagnetic wave propagation through stratified N-layer media. *J. Opt. Soc. Am. A* **2005**, *22*, 1143–1150. [CrossRef]
39. Zaghdoudi, J.; Maaloul, N.; Kanzari, M. Studies of Optical Properties of Symmetrical Quasi-Periodic Photonic Crystals. *Opt. Photon. J.* **2012**, *02*, 270–277. [CrossRef]
40. Fink, Y.; Winn, J.N.; Fan, S.; Chen, C.; Michel, J.; Joannopoulos, J.D.; Thomas, E.L. A Dielectric Omnidirectional Reflector. *Science* **1998**, *282*, 1679–1682. [CrossRef] [PubMed]
41. Liu, G.; Xuan, Y.; Han, Y.; Li, Q. Investigation of one-dimensional Si/SiO_2 hotonic crystals for thermophotovoltaic filter. *Sci. China Ser. E Technol. Sci.* **2008**, *51*, 2031–2039. [CrossRef]
42. Kumar, A.; Singh, P.; Pal, K.; Kumar, N.; Thapa, K.B. Broadband reflector of 1D photonic crystal containing TiO_2/SiO_2 material at visible region. In Proceedings of the AIP Conference, 3rd International Conference on Condensed Matter and Applied Physics (ICC-2019), Bikaner, India, 14 October 2019; Volume 2220, p. 020068.
43. Ren, J.; Xuan, H.; Liu, C.; Yao, C.; Zhu, Y.; Liu, X.; Ge, L. Graphene oxide hydrogel improved sensitivity in one-dimensional photonic crystals for detection of beta-glucan. *RSC Adv.* **2015**, *5*, 77211–77216. [CrossRef]